

2012

# Laser Induced Fluorescence Measurements Of Ion Velocity And Temperature Of Drift Turbulence Driven Sheared Plasma Flow In A Linear Helicon Plasma Device

S. Chakraborty Thakur

D. McCarren

T. Lee

N. Fedorczak

P. Manz

***See next page for additional authors***

# Laser induced fluorescence measurements of ion velocity and temperature of drift turbulence driven sheared plasma flow in a linear helicon plasma device

S. Chakraborty Thakur,[1,2] D. McCarren,[3] T. Lee,[2] N. Fedorczak,[1,2] P. Manz,[1,2] E. E. Scime,[3] G. R. Tynan,[1,2] and M. Xu[1,2]
[1]*Center for Momentum Transport and Flow Organization, University of California at San Diego, San Diego, California 92093, USA*
[2]*Center for Energy Research, University of California at San Diego, San Diego, California 92093, USA*
[3]*Department of Physics, West Virginia University, Morgantown, West Virginia 26506, USA*

(Received 14 March 2012; accepted 17 July 2012; published online 1 August 2012)

Using laser induced fluorescence (LIF), radial profiles of azimuthal ion fluid velocity and ion temperature are measured in the controlled shear de-correlation experiment (CSDX) linear helicon plasma device. Ion velocities and temperatures are derived from the measured Doppler broadened velocity distribution functions of argon ions. The LIF system employs a portable, high power (>300 mW), narrowband (~1 MHz) tunable diode laser-based system operating at 668.614 nm. Previous studies in CSDX have shown the existence of a radially sheared azimuthal flow as measured with time delay estimation methods and Mach probes. Here, we report the first LIF measurements of sheared plasma fluid flow in CSDX. Above a critical magnetic field, the ion fluid flow profile evolves from radially uniform to peaked on axis with a distinct reversed flow region at the boundary, indicating the development of a sheared azimuthal flow. Simultaneously, the ion temperature also evolves from a radially uniform profile to a profile with a gradient. Measurements in turbulent and coherent drift wave mode dominated plasmas are compared. © *2012 American Institute of Physics*. [http://dx.doi.org/10.1063/1.4742178]

## I. INTRODUCTION

The loss of particles and energy from the confinement regions of magnetically confined fusion plasma is believed to be driven by turbulent drift wave fluctuations. Drift waves are one of the fundamental modes in magnetized plasmas and detailed reviews of both the theoretical[1] and the experimental[2] aspects are available in literature. Drift waves can non-linearly drive poloidally and toroidally symmetric shear flows, called zonal flows, via the turbulent Reynolds stress.[3] Zonal flows in turn lead to transport barriers, de-correlation of the turbulence, and limit the absolute magnitude of the turbulence.[3] The interaction of turbulence and zonal flows has developed into one of the most active research topics in the physics of fusion related magnetized plasmas. Zonal flow studies in linear magnetized devices are underway to understand the generation mechanism of zonal flows and details of their interaction with drift wave turbulence.[4–12] In these experiments, it is important to be able to measure the radial profiles of the azimuthal plasma velocity in turbulence dominated plasma and compare them against drift wave dominated plasma without turbulence.

Previous studies[13] in the controlled shear decorrelation experiment (CSDX) have demonstrated a controlled transition to a turbulent state as the magnetic field (**B**) is increased from 300 G to 1000 G when the device is configured with insulating boundary conditions (IBC). With increasing **B**, the plasma drift wave fluctuations evolve from narrow-band coherent wavelike perturbations to a state of weak turbulence characterized by broadened frequency and wave number spectra. At a $\mathbf{B} = 1000$ G, the narrow-band coherent mode-like drift wave fluctuations (with a dominant m = 3 mode) coexist with the more broadband turbulent fluctuations; hence, we call this a state of weak turbulence. At magnetic fields higher than 800 G, studies in CSDX also show the presence of a turbulence driven azimuthally symmetric shear flow without any external sources of momentum input.[4,5] Nonlinear energy transfer analyses[8,14] have shown that for $\mathbf{B} = 1000$ G, the energy is transferred from the higher frequency ($f > 10$ kHz, $m = 3$ mode) turbulent fluctuations to the low frequency ($f < 1$ kHz, $m = 0$ mode) azimuthally symmetric shear flow. The azimuthally symmetric, low frequency sheared flow is driven by the high frequency turbulent plasma fluctuations and thus has the characteristics of a zonal flow.

Recent experiments on CSDX have also shown that, keeping all the source operation parameters the same, changing the end boundary conditions of the linear device from insulating (the standard boundary conditions) to conducting endplates can make it more difficult for the system to enter into a state of weak turbulence. Instead, in case of the conducting end-plate boundary conditions, even for $\mathbf{B} = 1000$ G, the plasma is completely dominated by narrow-band coherent mode-like drift wave fluctuations. The source parameters are kept constant during this change and thus within the uncertainty of the measurements the plasma density and the electron temperature remain the same for the IBC and the conducting boundary conditions (CBC). The results thus indicate that the endplate sheath conditions have an impact on the drift wave saturation and thus on the development of

 

the azimuthal shear flow. The effect of changing electrostatic boundary conditions, of a plasma device with open magnetic field lines, by biasing end rings is not new (Ref. 15 and the references therein). In this experiment, the end plates were simply changed from insulating to conducting, without any biasing. Thus, direct measurements of plasma ion fluid rotation in both IBC and CBC configurations are of interest to more fully understand the physics of turbulent-driven shear flow generation.

Laser induced fluorescence (LIF) is routinely employed in helicon[16–18] plasma sources to measure Doppler resolved velocity distribution functions (VDF) of argon ions, argon neutrals, helium neutrals, and xenon ions.[19–21] The full width at half maxima of the VDF represents the average temperature of the distribution and the shift of the peak of the distribution from a standard reference line gives the ion fluid velocity. Here, we use LIF on argon ions to measure radial profiles of the azimuthal velocity and the ion temperature of CSDX plasma in the turbulent and the quiescent regimes of both IBC and CBC configured CSDX discharges. These are the first LIF measurements on CSDX and to the best of our knowledge the first LIF measurements in helicon sources comparing turbulent and coherent drift wave mode like plasmas.

## II. EXPERIMENTAL APPARATUS

The experiments were carried out in a cylindrical magnetized helicon plasma device, the CSDX. The device is 2.8 m long with a vacuum chamber radius of 10 cm. Argon plasma is produced by a 13.56 MHz, 1500 watts helicon source having a radius of 4.5 cm and operated in the $m = 0$ helicon mode. The reflected power is less than 20 watts, and the chamber and the source are immersed in an axially uniform magnetic field of strength up to 1000 G. These experiments were performed at a neutral gas fill pressure of 3.2 mTorr. Details of the experimental device can be found elsewhere.[22] At the standard operating conditions, typical electron temperatures and plasma densities in CSDX, as measured by rf compensated,[23] cylindrical Langmuir probes are $T_e \approx 3$ eV and $n \approx 10^{13}$ cm$^{-3}$ respectively. Radial profiles of the standard plasma parameters like plasma density, electron temperature, and floating potential as the magnetic field is scanned from low ($\mathbf{B} = 400$ G) to high ($\mathbf{B} = 1000$ G) fields are shown in Ref. 13.

In the IBC experiments, the vacuum chamber terminated on a glass window, and the inner walls of the chamber which extended beyond the end of the array of magnets were covered with Teflon insulation. On the source end of the device, the inner wall of the flange that mated the glass bell jar of the 4.5 cm radius source to the 10 cm radius chamber was covered with an insulating layer of boron nitride. Thus, all possible regions where open magnetic field lines could come in contact with the chamber walls were insulated to prevent currents from flowing to and through the walls. In the CBC experiments, all insulators were removed and a grounded metal mesh was inserted at end of the chamber. In this configuration, the magnetic field lines exiting the chamber intersected conducting boundaries, allowing currents to flow through after passing through the standard plasma sheath at the boundaries. All external parameters for the helicon source, namely the neutral gas pressure, the gas flow rate, the forward and reflected power and the magnetic field, were kept constant in these experiments.

For LIF measurements, the light was injected using optics mounted on a manually controlled linear stage attached to a rectangular glass window at the top of the plasma chamber, 75 cm downstream from the helicon source. The translation stage moved the injected laser light to different radial locations. The emitted fluorescence light was collected through one of the ports of the chamber at the same axial location. The collection lenses were also placed on a manually controlled linear stage to ensure that the measured plasma volume and the solid angle of the measured emission remained constant for each radially localized measurement. Analysis of the Doppler broadened ion VDF (IVDF) provided measurements of the azimuthal ion fluid velocity and perpendicular ion temperature as a function of radial location in the plasma.

The LIF apparatus used for the experiment is shown schematically in Fig. 1. The laser was a Toptica TA 100 tunable diode laser consisting of a Littrow configuration master oscillator followed by a tapered amplifier. The laser has a line width of ~1 MHz and has a mode hop free tuning range

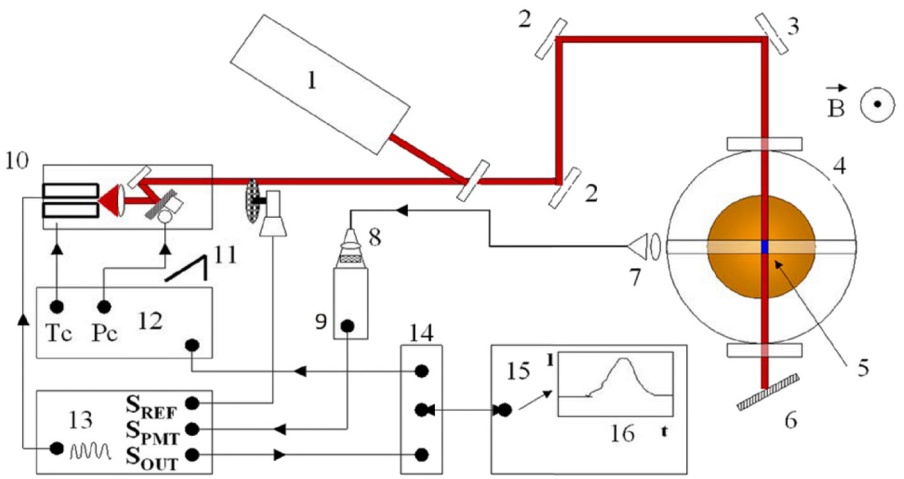


FIG. 1. Schematic of the LIF setup: 1. wavemeter, 2. laser beam steering optics, 3. laser beam injection mirror, 4. plasma chamber, 5. LIF volume, 6. laser beam dump, 7. collection optics, 8. interference filter, 9. photo-multiplier tube (PMT), 10. Toptica laser, 11. mechanical chopper, 12. laser controller, 13. lock-in amplifier, 14. data acquisition card, 15. laptop PC, 16. LIF signal (intensity vs. wavelength) for real time monitoring.

of more than 30 GHz. The coarse tuning range spans nearly 5 nm. For these measurements, the laser was tuned to 668.6138 nm; corresponding to $3d^4F_{7/2}$ to $4p^4D_{5/2}$ level transition in Ar II. The transition consists of circularly polarized sigma ($m = \pm 1$) and linearly polarized $\pi$ ($m = 0$) transitions. The laser is injected perpendicular to the magnetic field with its polarization axis aligned with the magnetic field. Thus, only the $\pi$ absorption lines are excited. For a magnetic field strength of 1 kG or less, the effect of the Zeeman splitting of the individual lines is much smaller than that of pure Doppler broadening and is ignorable in the analysis.[24,25] A single Gaussian fit gives results as good as a deconvoluted fit, within experimental errors. Optical isolators were inserted between the master oscillator and the amplifier and between the amplifier and the first optical component. A 10% sampling beam-splitter was used to sample the beam and the sampled light was coupled into a Bristol Instruments 621-VIS wavemeter for real-time wavelength monitoring. The wavelength was measured to an accuracy of $\pm 0.0001$ nm. The error in the measured azimuthal velocity due to this instrumental error is $\pm 45$ m/s. The other 90% of the laser light was mechanically chopped at a few kHz and transported to the plasma chamber by beam steering mirrors.

The fluorescent emission at 442.60 nm from the decay of $4p^4D_{5/2}$ state to the $4s^4P_{3/2}$ state was collected by another lens, collimated, and then coupled into an optical fiber. The light exiting the fiber some meters away was re-collimated, passed through a 1 nm wide filter centered at 443 nm, and measured with a visible light PMT. The intensity of the fluorescent emission from the excited state as a function of laser frequency gave a direct measurement of the IVDF in the region where the injected beam overlaps the collection volume. In this experiment, the spatial resolution of the LIF measurements was $\sim$3 mm. Since the PMT signal was composed of background spectral radiation, electron-impact-induced fluorescence radiation, and electronic noise, a Stanford Research SR830 lock-in amplifier was used for phase synchronous detection of the LIF signal. Lock-in amplification was essential since electron-impact-induced emission was several orders of magnitude larger than the fluorescence signal.

## III. RESULTS

To determine the Doppler broadened ion temperature and the Doppler shifted azimuthal velocity, a nonlinear least squares fitting routine fits the measured IVDF with a drifting Maxwellian distribution of the form

$$I_R(\nu) = I_R(\nu_o) e^{-m_i c^2 (\nu - \nu_o)^2 / 2kT_i \nu_o^2}, \quad (1)$$

where $\nu_o$ is the rest frame frequency of the absorption line, $m_i$ the ion mass, and $T_i$ the ion temperature. The full width at half maxima of the VDF is the ion temperature of the distribution and the shift of the peak of the distribution from the rest frame absorption frequency line gives the bulk perpendicular ion flow speed.

In Fig. 2, we show an example of the measured IVDF at two different experimental conditions: for a coherent drift mode dominated plasma and for a turbulent plasma. The scatter in the plots is due to small fluctuations in the emitted light intensity, proportional to plasma density fluctuations, within the experimentally probed volume of plasma. For the plasma state dominated by coherent drift waves, the scatter in the plots is minimal. The fluctuations are coherent and their contribution to the total signal averages to zero over the timescale of the measurement (for each wavelength step during the scan, 200 points were measured using the lock-in amplifier and averaged together to create each data point in the plot). For turbulent plasma, the fluctuations are aperiodic and persist even after averages over 500 measurements are

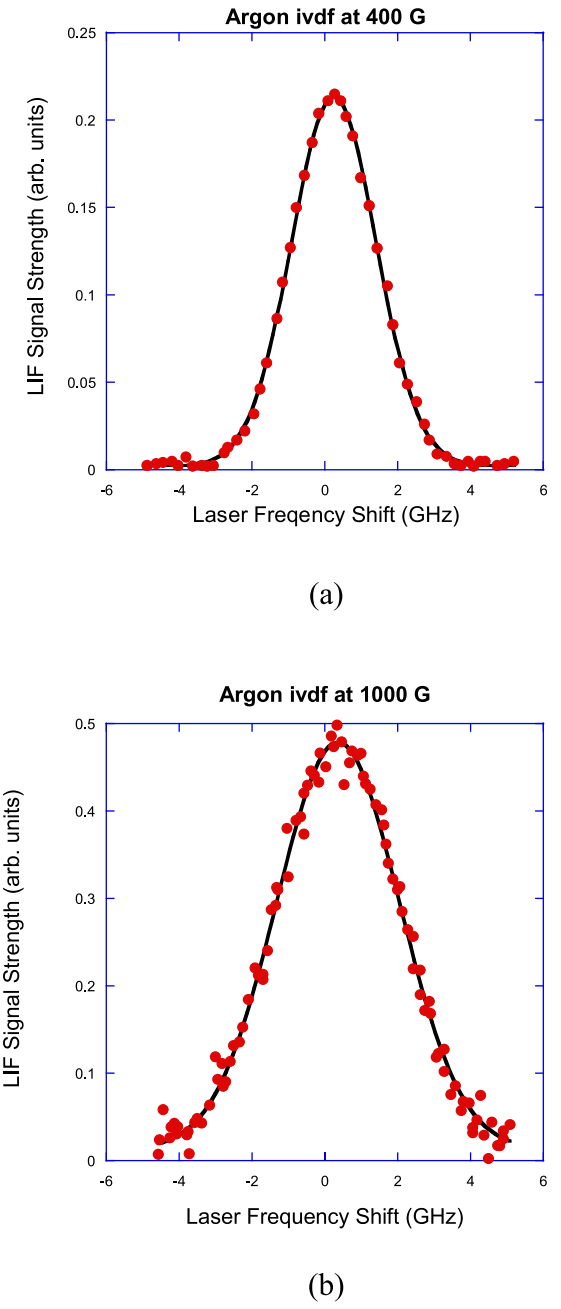


FIG. 2. Comparison of the Argon IVDF for (a) the quiescent (at 400 G) and (b) the turbulent (at 1000 G) plasma conditions. The noise in the turbulent plasma case persists even after averaging over many laser scans. For the plasma dominated by coherent drift wave modes (at 400 G) (a), the fluctuations average to zero over the time scale of the measurements.

performed. To obtain acceptable signal-to-noise levels in the measured IVDFs, multiple scans are recorded and then averaged together. For turbulent plasmas, recording several scans and averaging them together still did not reduce the scatter in the measured IVDF. Thus, the fluctuations in emission intensity are not normally distributed. The scatter in the plots provides a rough estimate of the plasma density fluctuation profile as we performed the experiment at different radial locations and for different parameters (both while changing the strength of the magnetic field and while changing the boundary conditions).

Fig. 3 shows the radial profiles of the azimuthal ion fluid velocity in the IBC configuration as the magnetic field is increased from 400 G to 1000 G. The behavior is consistent with flow measurements using two point time delay estimation (TDE) methods from camera data.[9] TDE methods depend critically on the ranges of frequency chosen for the calculations. Moreover, in TDE, the measured velocity is effectively a sum of both the bulk plasma fluid velocity and the phase velocity of the waves in the plasma. LIF, on the other hand yields the absolute fluid velocity of the ions and is unaffected by the phase velocity of any waves in the plasma. In these measurements, because the plasma density[14] decreased substantially beyond $r = 3.5$ cm, the errors in the density measurements increase for larger radii. Typical error in the azimuthal velocity measurements for $r < 3.5$ cm is $\sim \pm 30$ m/s and for $r > 3.5$ cm is $\sim \pm 60$ m/s. Towards the center of the plasma, the flow approximates solid body rotation; the azimuthal velocity increases linearly with distance. The time averaged flows are faster for larger magnetic fields. The azimuthal velocity reaches a maximum at around $r = 3$ cm and then rapidly decreases and undergoes a flow reversal for larger radii at the largest magnetic fields. The azimuthal ion velocity thus exhibits strong flow shear in the region from $r = 3.5$ cm to $r = 4.5$ cm. We find that both the peak velocity and the strength of the velocity shear (the radial gradient in the azimuthal velocity) increase with increasing magnetic field; concurrent with an increase in the turbulent fluctuation levels.

Fig. 4 shows the radial profiles of the perpendicular ion temperature as a function of the magnetic field. Typical error in the measurements for $r < 3.5$ cm is $\sim \pm 0.01$ eV and for $r > 3.5$ cm is $\sim \pm 0.03$ eV. For a magnetic field of 400 G, the ion temperature is nearly constant at $\sim 0.25$ eV at all radii. The ion temperature increases with increasing magnetic field. For the 1000 G magnetic field case, the peak ion temperature (on axis) is more than twice as large, $\sim 0.55$ eV, and there is significant gradient in the ion temperature from $r = 2.0$ cm to $r = 3.5$ cm. The ion temperature reaches a minimum at $r = 4.0$ cm, the same radius as the location of the strongest velocity shear. The development of a peak in the ion temperature profile is consistent with reduced transport of heat from the core of the plasma to the edge, i.e., an energy transport barrier.

In Figs. 5 and 6, we show the radial profiles of the azimuthal ion fluid velocity and the perpendicular ion temperature for the two different boundary conditions: IBC and CBC. We see that for the insulating boundary, the peak azimuthal velocity is almost twice of the conducting boundary case. As explained elsewhere, we have found that in the CBC the nonlinear interactions are not strong enough to push the system into a broadband turbulence regime. The reduced azimuthal flow observed is consistent with the hypothesis that the flows and turbulence are interrelated;

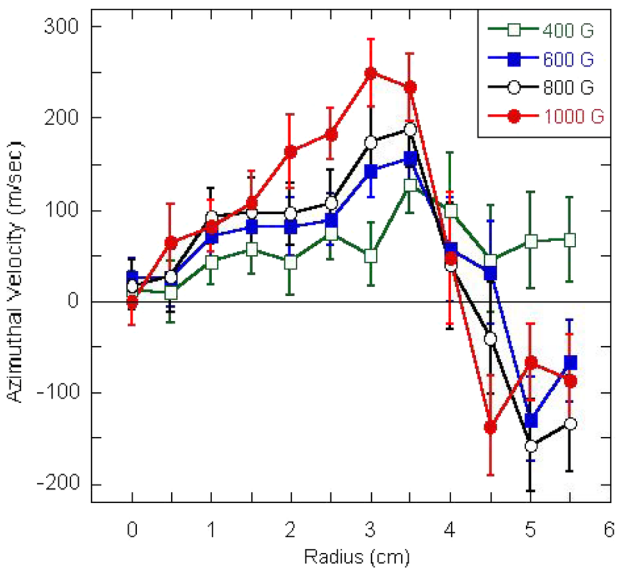


FIG. 3. Radial profiles of the azimuthal ion fluid velocity as the magnetic field is increased from 400 G (green empty squares), 600 G (blue solid squares), and 800 G (black empty circles) to 1000 G (red solid circles). Notice that both the peak velocity and the velocity shear increase with increasing magnetic field. Typical error in the measurements for $r < 3.5$ cm is $\sim \pm 30$ m/s and for $r > 3.5$ cm is $\sim \pm 60$ m/s. Results obtained for $P_{rf} = 1500$ W, argon gas pressure of 3.2 mTorr in IBC configuration.

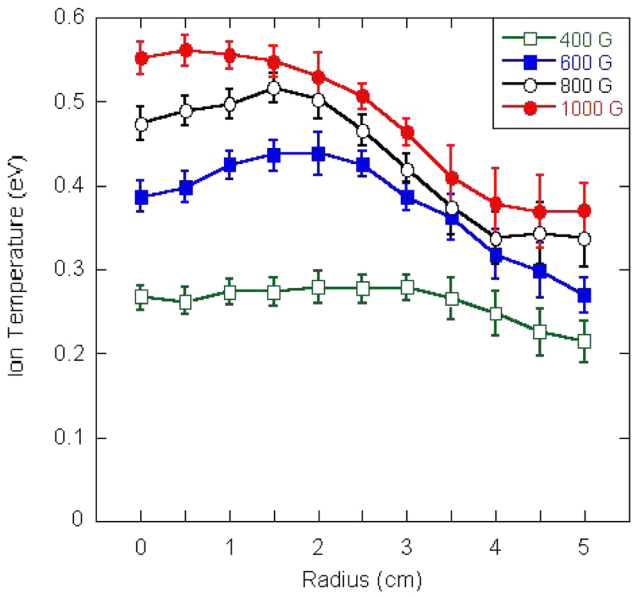


FIG. 4. Radial profiles of the perpendicular ion temperature as the magnetic field is increased from 400 G (green empty squares), 600 G (blue solid squares), and 800 G (black empty circles) to 1000 G (red solid circles). Notice that for the higher magnetic fields (which lead to turbulence driven sheared flows) the ion temperature profile steepens. Typical error in the measurements for $r < 3.5$ cm is $\sim \pm 0.01$ eV and for $r > 3.5$ cm is $\sim \pm 0.03$ eV. Results obtained for $P_{rf} = 1500$ W, argon gas pressure of 3.2 mTorr in IBC configuration.

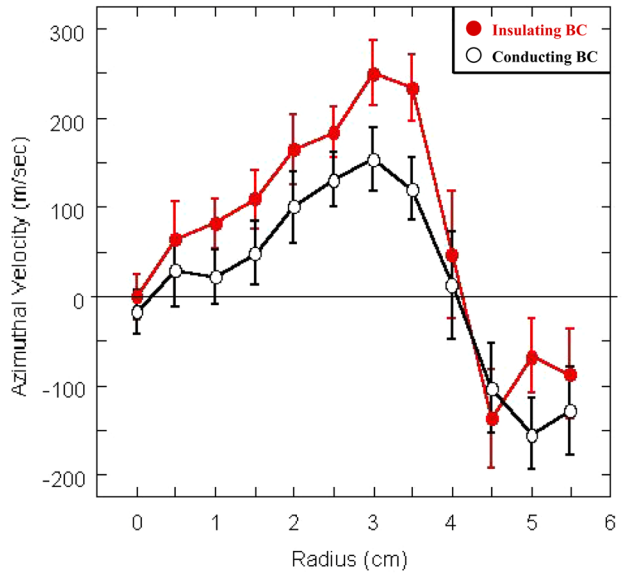


FIG. 5. Radial profiles of the azimuthal ion fluid velocity for the insulating boundary conditions (red solid circles) and the conducting boundary conditions (black empty circles). Results obtained for $B = 1000\,G$, $P_{rf} = 1500\,W$, argon gas pressure of 3.2 mTorr. Positive velocity here corresponds to flow in the electron diamagnetic drift direction.

similar to what is observed during the magnetic field magnitude scan. Moreover, from the radial profiles of the ion temperature, we see that even although the on-axis temperature is the same for the two boundary conditions, the ion temperature gradient is much smaller in the CBC, a result that is consistent with an energy transport barrier developing for the insulating boundary with stronger flow shear.

In CSDX, the fluid plasma flows are in the electron diamagnetic drift direction, as measured by LIF, Mach probes, and time delay estimation methods from probes or camera images. The plasma potential as measured by rf-compensated

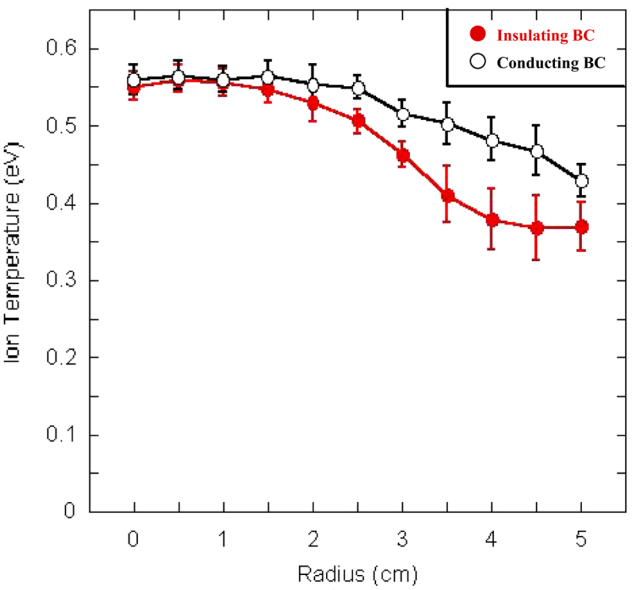


FIG. 6. Radial profiles of the perpendicular ion temperature for the insulating boundary conditions (red solid circles) and the conducting boundary conditions (black empty circles). Results obtained for $B = 1000\,G$, $P_{rf} = 1500\,W$, argon gas pressure of 3.2 mTorr.

swept Langmuir probes is hollow; the corresponding $\mathbf{E} \times \mathbf{B}$ flow is also in the electron drift direction. The radial profile of the $\mathbf{E} \times \mathbf{B}$ flow is similar to that measured by LIF, but the peak $\mathbf{E} \times \mathbf{B}$ velocity is larger in magnitude. Using the measured radial profiles of ion temperature and the density gradient, the contribution of the ion diamagnetic drift to the net measured LIF velocity is calculable. We find that in CSDX, the LIF measurements are effectively a vector sum of the $\mathbf{E} \times \mathbf{B}$ velocity and the ion diamagnetic drift. The $\mathbf{E} \times \mathbf{B}$ drift velocity is opposite in direction to that of the ion diamagnetic drift and larger in magnitude; hence, the net fluid plasma flow is in the electron diamagnetic drift direction. In Fig. 7, we show the radial profiles of the $\mathbf{E} \times \mathbf{B}$ flow, LIF velocity, and the ion diamagnetic drift. We see that the sum of the $\mathbf{E} \times \mathbf{B}$ flow and the ion diamagnetic drift is similar to the LIF measurements.

## IV. DISCUSSION

A detailed study of the effects of the boundary conditions on the drift turbulence and shear flow generation has been prepared and will be published elsewhere, but the observations can be put into a physics context by considering how electrical currents move within the plasma. For drift waves, due to quasi-neutrality, the divergence of the parallel current is balanced by that of the perpendicular polarization current. This balance determines the effective radial momentum flux, i.e., the Reynolds stress[26] and thus impacts the development of sheared azimuthal flows. The dynamics of drift wave turbulence can be described by two coupled dimensionless nonlinear equations describing the evolution of the kinetic energy and the internal energy.[27] There are two main nonlinearities; one acting on the vorticity fluctuations (kinetic energy) and the other acting on the density perturbations (internal energy). The vorticity fluctuations, related to the fluctuations in the perpendicular polarization current, are referred to as the polarization drift nonlinearity. The hydrodynamic derivative in the electron continuity equation gives rise to the other nonlinearity in the density fluctuations, referred to as the $\mathbf{E} \times \mathbf{B}$ drift nonlinearity. These two nonlinearities are responsible for the redistribution of kinetic and internal energy between different scales[28] such that a dual cascade, typical of two-dimensional turbulence, can develop. Changes in the parallel current also affect the nonlinear energy transfer from smaller to larger scales, i.e., the inverse energy cascade and thus the development of the sheared azimuthal flow. In case of CBC, reduced polarization drift nonlinearity decreases the inverse energy transfer coupling mechanisms, hence hindering the transition to broadband turbulence. It has been previously shown how this term plays a crucial role in the transition to turbulence in the IBC configuration.[14]

The reduction in the radial polarization current through the plasma can also be understood in terms of radial currents allowed to flow through the conducting end plates which flow in parallel to the radial current through the plasma. In the CBC configuration, the parallel current entering the end plates after crossing the sheaths can radially move through the conducting end plates and thus reducing the net effective

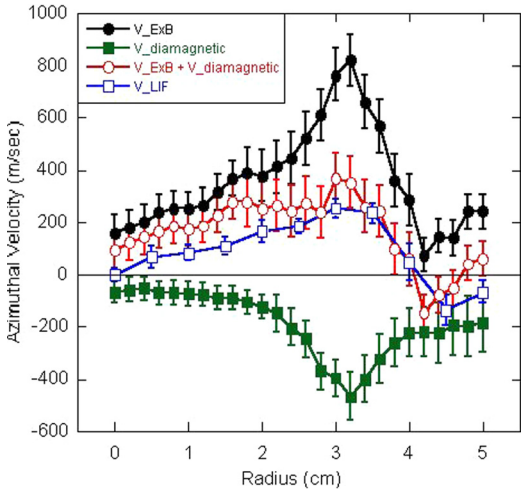


FIG. 7. Comparison of the radial profiles of the E × B drift velocity (black solid circles), LIF velocity (blue empty squares), the ion diamagnetic drift (green solid squares), and the sum (red empty circles) of the E × B drift and the ion diamagnetic drift velocities, for the insulating boundary conditions at B = 1000 G, $P_{rf}$ = 1500 W, argon gas pressure of 3.2 mTorr.

radial current flowing through the plasma or, equivalently, reduce the Reynolds stress. This end-plate loss term vanishes in the IBC configuration as there is no net current flow into the insulated end plates. Thus, it is as if the conducting end plates effectively reduce, if not completely "short circuit," the radial currents in the plasma and carry away any radial current needed to enforce $\nabla \cdot \mathbf{J} = 0$ through the end plates. In a single-fluid picture of the system, the Lorentz force arising from these radial current flowing through the plasma is what sustained the azimuthal shear flow. Thus, short circuiting these currents reduces or eliminates the origin of the shear flow.

## V. CONCLUSIONS

Both the magnetic field scan and the boundary condition changes indicate that as the plasma becomes more turbulent, the velocity shear increases in magnitude and simultaneously the ion temperature profile steepens in CSDX. These LIF measurements provide the first unambiguous measurement of the azimuthal ion fluid velocities as the system is driven to the turbulent state, and they show that the endplate boundary conditions are an important effect impacting the transition to drift wave turbulence and the development of sheared flows. A detailed study of this physics has been carried out and is being reported in a separate publication. Equally significant are the spatially resolved perpendicular ion temperature measurements. The ion temperature profile measurements also provide the data needed to compute the ion-ion collisional viscosity profiles, which are needed for understanding the details of the momentum balance between the Reynolds stress and the flow damping. Further work is being done on the details of the momentum balance including these new ion temperature profiles and will be published elsewhere. The only other experimentally relevant parameter for turbulent momentum balance that is not yet measured in CSDX is the radial profile of the neutral gas density. Although calculations suggest that the effect of spatial variations in the neutral gas density is smaller than the effects of spatial variations in the ion temperature, it would be useful to obtain actual measurements of the neutral density profile. In future experiments, we intend to measure the radial profile of neutral gas density in CSDX with LIF.[29,30]

## ACKNOWLEDGMENTS

We would like to thank Sandy Rosas and Leo Chousal for their help and advice while procuring and building parts for setting up the LIF diagnostic. This work was supported by NSF Award No. PHY-0611571 and PHY-0918526.

[1]W. Horton, Rev. Mod. Phys. **71**, 735 (1999).
[2]G. R. Tynan, A. Fujisawa, and G. Mckee, Plasma Phys. Controlled Fusion **51**, 113001 (2009).
[3]P. H. Diamond, S.-I. Itoh, K. Itoh, and T. S. Hahm, Plasma Phys. Controlled Fusion **47**, R35 (2005).
[4]C. Holland, J. H. Yu *et al.*, Phys. Rev. Lett. **96**, 195002 (2006).
[5]G. R. Tynan, C. Holland, J. H. Yu, A. James, D. Nishijima, M. Shimada, and N. Taheri, Plasma Phys. Controlled Fusion **48**, S51 (2006).
[6]Z. Yan, J. H. Yu, C. Holland, M. Xu, S. H. Müller, and G. R. Tynan, Phys. Plasmas **15**, 092309 (2008).
[7]M. Xu, G. R. Tynan, C. Holland, Z. Yan, S. H. Muller, and J. H. Yu, Phys. Plasmas **16**, 042312 (2009).
[8]M. Xu, G. R. Tynan, C. Holland, Z. Yan, S. H. Muller, and J. H. Yu, Phys. Plasmas **17**, 032311 (2010).
[9]Z. Yan, G. R. Tynan, C. Holland, M. Xu, S. H. Muller, and J. H. Yu, Phys. Plasmas **17**, 032302 (2010).
[10]Y. Nagashima *et al.*, Phys. Plasmas **16**, 020706 (2009).
[11]T. Windisch, O. Grulke, and T. Klinger, J. Nucl. Mater. **390**, 395 (2009).
[12]T. A. Carter and J. E. Maggs, Phys. Plasmas **16**, 012304 (2009).
[13]M. J. Burin, G. R. Tynan, G. Y. Antar, N. A. Crocker, and C. Holland, Phys. Plasmas **12**, 052320 (2005).
[14]P. Manz, M. Xu, S. C. Thakur, and G. R. Tynan, Plasma Phys. Controlled Fusion **53**, 095001 (2011).
[15]A. Mase, A. Itakura, M. Inutake, K. Ishii, J. H. Jeong, K. Hattoti, and S. Miyoshi, Nucl. Fusion **31**, 1725 (1991).
[16]R. W. Boswell, Plasma Phys. Controlled Fusion **26**, 1147 (1970).
[17]A. B. Altukhov, E. Z. Gusakov, M. A. Irzak, M. Krämer, B. Lorenz, and V. L. Selenin, Phys. Plasmas **12**, 022310 (2005).
[18]J. G. Kwak, S. J. Wang, S. K. Kim, and S. Cho, Phys. Plasmas **13**, 074503 (2006).
[19]A. M. Keesee, R. Boivin, and E. E. Scime, Rev. Sci. Instrum. **75**, 4091 (2004).
[20]A. Aanesland, L. Liard, G. Leray, J. Jollyand, and P. Chabert, Appl. Phys. Lett. **91**, 1 (2007).
[21]G. Severn, L. Dongsoo, and N. Hershkowitz, Rev. Sci. Instrum. **78**, 116105 (2007).
[22]G. R. Tynan, A. D. Bailey III *et al.*, J. Vac. Sci. Technol. A **15**, 2885 (1997).
[23]I. D. Sudit and F. F. Chen, Plasma Sources Sci. Technol. **3**, 162 (1994).
[24]R. F. Boivin, *Zeeman Splitting for LIF Transitions and De-Convolution Technique to Extraction Temperatures, PL-050* (West Virginia University, Morgantown, USA, 2002).
[25]R. F. Boivin, *Study of The Different Line Broadening Mechanisms for the Laser Induced Fluorescence Diagnostic of the HELIX and LEIA Plasmas, PL-039* (West Virginia University, Morgantown, USA, 2002).
[26]P. H. Diamond and Y.-B. Kim, Phys. Fluids B **3**, 1626 (1991).
[27]A. Hasegawa and M. Wakatani, Phys. Rev. Lett. **50**, 682 (1983).
[28]P. Manz, M. Ramisch, and U. Stroth, Plasma Phys. Controlled Fusion **51**, 035008 (2009).
[29]A. Keesee and E. E. Scime, Rev. Sci. Instrum. **77**, 10F304 (2006).
[30]A. Keesee and E. E. Scime, Plasma Sources Sci. Technol. **16**, 742 (2007).